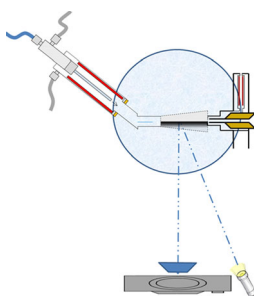


# Characterization of a Direct Sample Analysis (DSA) Ambient Ionization Source

Gregory T. Winter, Joshua A. Wilhide, William R. LaCourse

University of Maryland, Baltimore County, Baltimore, MD 21250, USA



**Abstract.** Water cluster ion intensity and distribution is affected by source conditions in direct sample analysis (DSA) ionization. Parameters investigated in this paper include source nozzle diameter, gas flow rate, and source positions relative to the mass spectrometer inlet. Schlieren photography was used to image the gas flow profile exiting the nozzle. Smaller nozzle diameters and higher flow rates produced clusters of the type  $[H + (H_2O)_n]^+$  with greater  $n$  and higher intensity than larger nozzles and lower gas flow rates. At high gas flow rates, the gas flow profile widened compared with the original nozzle diameter. At lower flow rates, the amount of expansion was reduced, which suggests that lowering the flow rate may allow for improvements in sampling spatial resolution.

**Keywords:** Schlieren photography, Ambient ionization, Desorption atmospheric pressure chemical ionization, DAPCI, Direct sample analysis, Water clusters

Received: 11 November 2014/Revised: 21 April 2015/Accepted: 25 April 2015/Published Online: 20 June 2015

## Introduction

The direct sample analysis (DSA) ionization source represents a modified form of atmospheric pressure chemical ionization (APCI), operating on the basis of a corona discharge in nitrogen at atmospheric pressure. Other common ambient ionization sources operating on the principles of APCI include desorption atmospheric pressure chemical ionization (DAPCI) [1] and atmospheric solids analysis probe (ASAP) [2]. DAPCI and ASAP sources have been used for a variety of analyses, including explosives [3], food products [4], pharmaceuticals [5, 6], and samples of biological origin [7–10]. These APCI type sources are thought to produce analyte ions primarily through a thermal desorption and proton transfer type mechanism involving the formation of protonated water clusters [11, 12], through the well-known APCI ionization cascade [13, 14].

Presented in this work is an examination of various DSA source conditions and their effect on water cluster ion formation. Variables examined include nozzle internal diameter, source position relative to the mass spectrometer inlet (vertical and horizontal), and gas flow rate. Water cluster ion formation was monitored by a single quadrupole mass spectrometer.

Schlieren photography was used to observe and evaluate how changes in source conditions impact the gas flow profile produced by the source, and how the gas flow profile relates to ion transmission at the mass spectrometer interface.

Schlieren photography allows for the visualization of transparent media based on differences in refractive index, causing a distortion of light, within that media. Despite the small difference in refractive index between nitrogen and air [15], the increased temperature of the nitrogen gas used by the DSA relative to the cooler surrounding air provides a significant-enough change in refractive index for the gas flow to be observed using schlieren photography.

In the field of ambient mass spectrometry, schlieren photography has been used to study helium flow and mass transport properties of a flowing atmospheric pressure afterglow source [16–18] and to visualize flow from a direct analysis in real time source coupled with atmospheric pressure drift tube ion mobility spectrometry [19].

## Experimental

### *Direct Sample Analysis (DSA)*

The DSA (PerkinElmer, Waltham, MA, USA) consists of a combined ionization source and sampling platform. A schematic representation of the source can be found in Fig. 1; in this configuration the source is open to the laboratory environment.

**Electronic supplementary material** The online version of this article (doi:10.1007/s13361-015-1175-1) contains supplementary material, which is available to authorized users.

Correspondence to: William LaCourse; e-mail: lacourse@umbc.edu

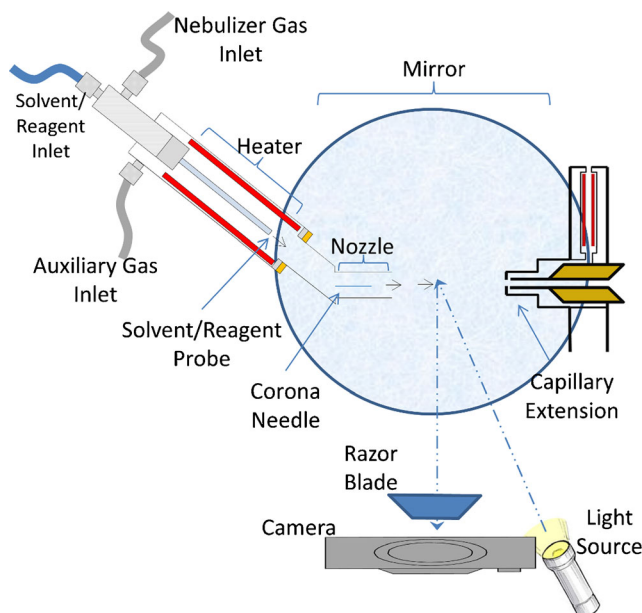


Figure 1. DSA source with schlieren experimental setup

The source is composed of a heating element and thermocouple, nebulization and auxiliary gas inlets, reagent/solvent introduction probe, and corona discharge electrode. Nitrogen is introduced into the system, where it is heated and directed past the discharge electrode that is arranged in a wire-cylinder configuration. This cylinder also functions as the nozzle, to direct the flow of gas. The discharge electrode is oriented at a 45° angle relative to the heater and gas assembly. Operating the DSA requires the use of an extension for the inlet capillary. The extension is made from stainless steel with a length of 34 mm and an internal diameter of 2 mm. Under standard conditions, the source can be adjusted so that the distance between the nozzle and inlet of the mass spectrometer is between 10 and 25 mm. The source is attached to a robotic sampling platform that can introduce samples via a 13-spot stainless steel mesh screen. Each mesh spot forms a circular sampling region with a diameter of 9.5 mm.

The source was operated in positive mode. To initiate and maintain the positive corona discharge, a current of 5  $\mu\text{A}$  was applied to the electrode and the voltage was allowed to vary to maintain the current. The heater element was set to 300°C. No additional water or reagents were added to the system. The relative humidity of the laboratory, measured using a digital sling psychrometer (General, New York, NY, USA), varied between 56% and 58%. Nitrogen gas was supplied from an in-house nitrogen generation system (Parker, Cleveland, OH, USA) at 80 pounds per square inch (psi) unless otherwise stated. Mass flow control was not used. Supplied nitrogen was dried to a dew point of  $-50^\circ\text{C}$  and had a purity of  $\geq 99.0\%$ . An anemometer (Extech, Nashua, NH, USA) was used to measure the linear velocity of the gas flow from each nozzle.

### Mass Spectrometer

A PerkinElmer SQ 300 single quadrupole mass spectrometer was used to monitor background reagent ions as source conditions were changed. The mass spectrometer was operated in positive mode and calibrated with Agilent APCI-L low concentration tuning mix (Agilent Technologies, Santa Clara, CA, USA) prior to data acquisition. Tuning parameters established by the mass spectrometer resulted in an effective mass range of 30–100 Da. The capillary entrance and endplate voltages were both set to  $-1000\text{ V}$ . A nitrogen curtain gas flowing at 2  $\text{L}\cdot\text{min}^{-1}$  at  $25^\circ\text{C}$  was used. All parameters of the source were optimized through the mass spectrometer software, SQ 300 MS Driver ver. 2.2.

### Nozzles

The DSA is not manufactured with interchangeable source nozzles; however, reducing nozzle diameter is investigated here to determine the feasibility of improving sampling spatial resolution. Four nozzles with decreasing internal diameters were utilized. The stock nozzle from the source was replaced with one that had external threads that served as the base to mount additional nozzles. Components for the nozzles consisted of stainless steel Swagelok gas fittings (Swagelok, Solon, OH, USA) and HPLC ferrules and tubing (IDEX Health and Science, Oak Harbor, WA, USA). Nozzle 1 had the same internal diameter as the stock nozzle, 4.8 mm; nozzles 2, 3, and 4 had smaller internal diameters of 3.2, 1.5, and 0.5 mm, respectively. Photographs of the nozzles can be found in Figure S1 of the supplementary material [ESM1].

### Schlieren Experimental Setup

The schlieren experimental setup was arranged in a simple, cost effective, single mirror off-axis configuration [20, 21]. A schematic representation of the schlieren experimental setup in relation to the source can be found in Fig. 1. The concave spherical mirror, (Edmund Optics, Barrington, NJ, USA), had a diameter of 150 mm and a 1500 mm focal length. The light source consisted of a LED flashlight (EAGTAC, East Wenatchee, WA, USA) producing 200 lumens, which was modified to only allow light through a hole approximately 0.6 mm in diameter. The light source was placed off-axis at twice the focal length of the mirror. A razor blade was used to create a knife edge at the focal point just before the camera, a Canon EOS Rebel T2i (Canon, Melville, NY, USA) with a 300 mm telephoto lens. The source was placed directly in front of the mirror in the test region. The degree of light cutoff was controlled by moving the razorblade vertically in the path of the light. The amount of cutoff was approximately 50%. For the schlieren experiments, the source was removed from the sampling platform to allow for proper positioning of the mirror.

## Results and Discussion

### *The Effect of Nozzle Diameter on Water Cluster Ions at a Fixed Distance*

Three primary water clusters were observed in the established mass window at  $m/z$  37, 55, and 73 corresponding to protonated clusters of  $[\text{H} + (\text{H}_2\text{O})_n]^+$  where  $n = 2, 3,$  and  $4,$  respectively. For this experiment, the distance was fixed at 25 mm, the maximum adjustable distance, to allow clear visualization of the gas flow as well as access to change the nozzles.

Schlieren photographs of the gas stream produced by each of the four nozzles are shown in Fig. 2. The gas flow profile from all nozzles expanded at the mass spectrometer inlet, relative to the original nozzle diameter. As nozzle internal diameter was reduced, the streams became more confined; however, no nozzle produced a gas stream of uniform diameter. From the schlieren photographs, spray half angles of  $24^\circ, 21^\circ, 10^\circ,$  and  $7^\circ$  were estimated for nozzles 1–4, respectively.

The relationship between nozzle internal diameter and water cluster intensity and distribution is represented graphically in Fig. 3a. As nozzle internal diameter decreased, the summed intensity of the three observed water clusters increased, reaching a maximum intensity with nozzle 3, followed by a drop in intensity with nozzle 4. This trend was also followed by the linear velocity of the gas exiting each nozzle. The linear velocity increased from 2.2 to 3.0 to  $4.3 \text{ m}\cdot\text{s}^{-1}$  for nozzles 1, 2, and 3 respectively, with a drop in velocity to  $1.6 \text{ m}\cdot\text{s}^{-1}$  for nozzle 4.

The reduction in linear velocity observed with nozzle 4 has been attributed to gas leaks within the system that were observed in the schlieren photographs (Supplementary Figure S2). These leaks are likely caused by the increased pressure within the system attributable to the small diameter nozzle. The source may not be gas tight, and there are points within its construction where gaps may exist, such as the

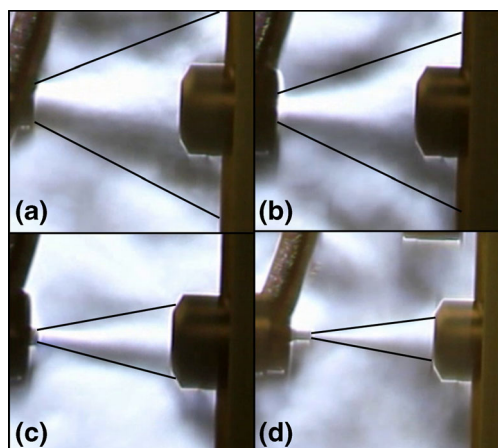


**Figure 2.** Schlieren photographs of nozzles 1–4 at a fixed distance of 25 mm between source and inlet (a) nozzle 1, internal diameter 4.8 mm, (b) nozzle 2, internal diameter 3.2 mm, (c) nozzle 3, internal diameter 1.5 mm, (d) nozzle 4, internal diameter 0.5 mm

ceramic insulators that form the electrode body and the joint between the heater body and electrode. Linear velocity alone does not account for the observed trends in water cluster ion intensity and distribution. For example, nozzles 1 and 4 produced comparable overall cluster intensities despite having different linear gas velocities. An additional factor in the production of water clusters is the density of the initial reactive nitrogen species within the nitrogen gas flow that begin the APCI cascade. As nozzle internal diameter is reduced, the density of the nitrogen species within the gas stream increases, resulting in the production of more water clusters in a reduced volume. The higher concentration shifts the equilibrium of the APCI clustering reaction to larger clusters. This is evident in the data as the base peak in the spectra for nozzle 1 is  $m/z$  37; however, for nozzles 2–4 the base peak becomes  $m/z$  55. Additionally, comparing cluster intensity produced by nozzles 1, 2, and 3,  $m/z$  37 consistently decreases in intensity while  $m/z$  55 and 73 increase.

Another effect of decreasing nozzle internal diameter is the reduction in additional background signal. For example,  $m/z$  42, attributed to the protonated form of acetonitrile from surrounding HPLC instruments, appears as a dominant peak in spectra produced by nozzle 1. However, the intensity of  $m/z$  42, also included in Fig. 3a, gets smaller and almost disappears as nozzle internal diameter is reduced.

The shift in equilibrium to larger clusters results in a higher overall proton affinity for the reagent ion system. It is known that as protonated water clusters increase in size, so too does the proton affinity (PA) of the cluster [22–24]. The calculated PAs of the observed clusters,  $n = 2, 3,$  and  $4$  are 832, 888, and 919  $\text{kJ}\cdot\text{mol}^{-1}$ , respectively [23]. Therefore, it is unlikely that proton transfer to acetonitrile, PA 779  $\text{kJ}\cdot\text{mol}^{-1}$  [25], occurs from any of these species.

Although not observed under these mass spectrometer tuning parameters, the presence and response to changes in nozzle diameter of  $[\text{H} + (\text{H}_2\text{O})_n]^+$ ,  $n = 1$ , can be inferred from the response of  $m/z$  42. The proton affinity of water, 691  $\text{kJ}\cdot\text{mol}^{-1}$  [25], is lower than that of acetonitrile; therefore, proton transfer from  $[(\text{H}_3\text{O})]^+$  to acetonitrile is the likely route for ionization. Following the trend of shifting cluster equilibrium, the amount of formed  $[(\text{H}_3\text{O})]^+$ , and subsequently the amount of ionized acetonitrile, decrease with decreasing nozzle internal diameter. As a result, larger water clusters are produced in greater number, reducing the amount of acetonitrile that is ionized and detected. Additionally, the reduction in intensity of the acetonitrile signal may also result from the increased velocity and in the force of the nitrogen gas stream, which serves to limit the influx of atmospheric volatiles.

### *Distribution and Intensity of Clusters between Source and Inlet*

To investigate the intensity and distribution of the clusters over the adjustable distance, the source was moved linearly relative to the inlet of the mass spectrometer. The nozzle of the source was positioned in line with the inlet of the mass spectrometer at

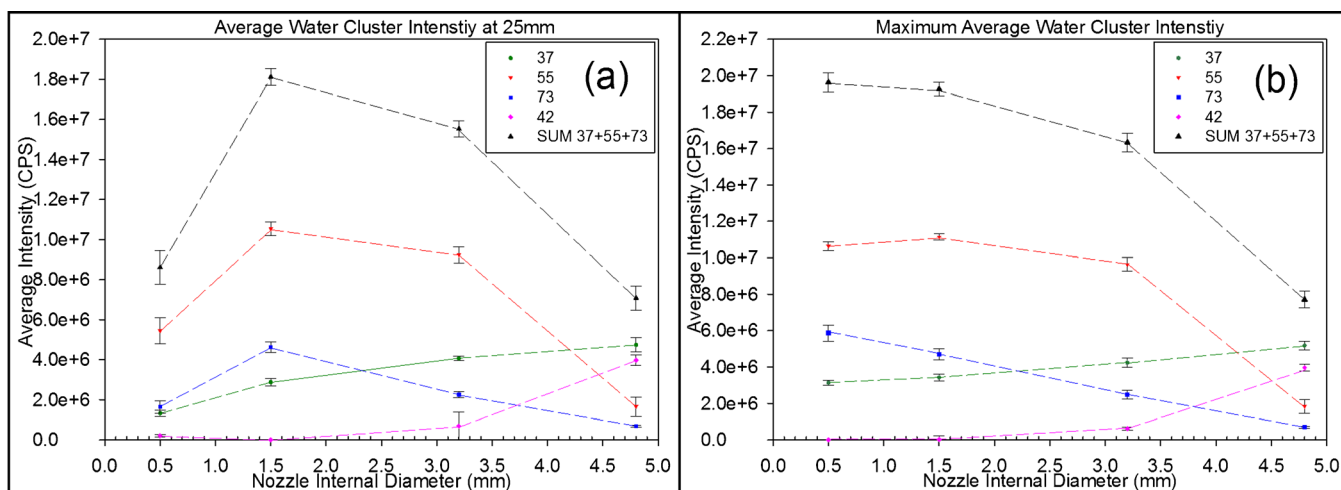


**Figure 3.** (a) Plot of nozzle internal diameter with the corresponding ion intensity at a fixed distance of 25 mm between source and inlet, (b) plot of nozzle internal diameter and corresponding ion intensity at the distance where maximum signal was observed (error bars represent the variation in recorded signal as  $\pm 1$  standard deviation of 20 spectra averaged for each point. Dashed lines are added to aid in visualizing the trends and do not represent a mathematical fit)

an initial distance of 10 mm. The source was held at this position for 1 minute to allow the signal to stabilize, then moved away from the inlet at approximately  $10\text{mm}\cdot\text{min}^{-1}$  to a position of 25 mm. Over the distance of 10 to 25 mm the cluster ion signal for nozzles 1, 2 and 3 increased until a maximum was reached. Maximum signal was considered to be the point at which the sum of the intensities of the clusters was greatest. Nozzles 1 and 2 reached maximum signal approximately 22 mm from the inlet while nozzle 3 was closer at approximately 19 mm. Nozzle 4 exhibited maximum intensity at the initial 10 mm distance, with a decrease in signal as the distance increased to 25 mm. Nozzles 1 and 2 likely have the same maximum intensity distance due to their similar spray half angles, which produces a similar volume of gas at that distance. Extracted ion chromatograms (EICs) can be found in Supplementary Figures S3–S6.

A plot of the maximum signal intensities at the observed location for each nozzle is shown in Fig. 3b. Overall, nozzles 3 and 4 produce comparable maximum ion intensity, but at different distances with a different distribution of water clusters. Supporting the shift in clustering equilibrium,  $m/z$  37 decreased with decreasing nozzle diameter as larger clusters are formed. The base peak for nozzles 2, 3 and 4 remains  $m/z$  55, however, the intensity of  $m/z$  55 begins to drop with nozzle 4. Despite the drop in intensity of  $m/z$  37 and 55, the intensity of  $m/z$  73 increased from nozzle 3 to 4, indicating that the equilibrium continues to shift toward larger clusters. Also plotted in Fig. 3b is the intensity of  $m/z$  42, which again decreases with decreasing nozzle diameter until it is no longer detected in the spectra of nozzles 3 and 4.

The observed initial rise in signal for nozzles 1–3 is likely due to increased mixing with the atmosphere as the gas volume increased between the nozzle and inlet. Nozzle 4 had the lowest gas linear velocity, which resulted in reduced mass transport to

the mass spectrometer at the larger distances and, therefore, no increase in signal was observed.

### *Distribution and Intensity of Clusters within the Vertical Gas Profile*

The schlieren photographs show that the gas flow profile produced by the nozzles is not uniform and expands as it reaches the mass spectrometer. In order to investigate the intensity and distribution of water cluster ions at different positions within the gas stream, the source was moved vertically relative to the inlet of the mass spectrometer. Initially, the source was positioned at 10 mm above center. The source was then lowered in 5 mm increments to 10 mm below center. For each nozzle, the source was placed at the distance where maximum signal was observed.

Figure 4 contains the schlieren photographs and corresponding mass spectra for nozzle 2 at different height positions. Despite the wider gas flow profile and visible overlap of the inlet at the off-centered positions, maximum water cluster ion intensity was observed when the source was centered. Nozzle 2 showed a large disparity in cluster ion intensity between the centered and off-centered positions, with  $m/z$  55 decreasing approximately 40-fold in intensity. Additionally, at the  $\pm 5$  mm position the distribution of water clusters shifts back to smaller clusters with an increase in intensity of  $m/z$  42. At the  $\pm 10$  mm, no signal was observed for any nozzle. The effect at the edges is not as drastic with nozzle 1; the intensity of  $m/z$  55 is approximately 2- to 3-fold lower when the source is  $\pm 5$  mm off-center. At the  $\pm 5$  mm position, very little signal is observed from nozzle 3, and no signal is observed for nozzle 4. For all nozzles, the overall background and total ion intensity is lower in the off-centered positions. Mass spectra of the remaining nozzles can be found in Supplementary Figures S7–S9.



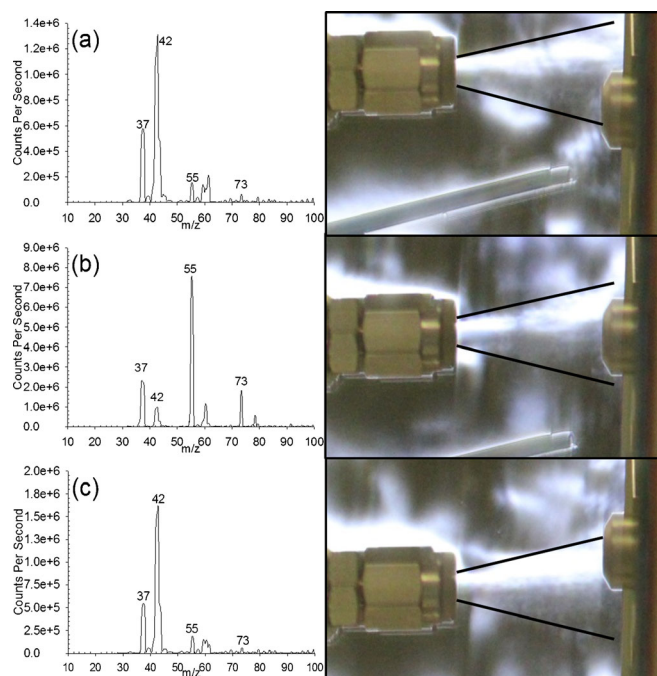


**Figure 4.** Schlieren photographs and corresponding mass spectra for nozzle 2 (3.2 mm) at (a) +5 mm off-center, (b) 0 mm off-center, (c) -5 mm off-center

The observed trends show that even with the large nozzles and wide gas flow profiles, the reactive nitrogen species and ultimately the bulk of the produced water clusters remain in the center of the gas flow. Sample placement and alignment on the mesh screens used with the DSA will become more critical as nozzle diameter is reduced.

### *Effect of Gas Flow Rate on Water Cluster Ions*

For this experiment, the source was positioned at the location where maximum water cluster ion signal was observed. Gas flow rate was reduced by decreasing the nitrogen pressure in discrete increments of 10 psi every minute from 80 to 20 psi. As was expected, the general overall trend was a decrease in signal intensity for each ion with decreasing flow rate. The EICs for the water cluster ions produced by nozzles 1 and 3 are shown in Fig. 5, along with schlieren photographs at 80 and 20 psi of supplied nitrogen.

As flow rate is reduced, the amount of reactive nitrogen species being produced also decreases. The reduction in reactive nitrogen species resulted in decreasing water cluster production and a change in cluster equilibrium. Indicative of the shift to smaller clusters, as the flow rate was reduced with nozzle 1, the intensity of each of the observed water clusters decreased while the intensity of  $m/z$  42 increased. From this increase in  $m/z$  42, it is inferred that the amount of  $[(\text{H}_3\text{O})]^+$  is also increasing. The intensity of  $m/z$  42 reaches a maximum, then decreases as the lower flow rates result in reduced mass transport to the mass spectrometer.

Spectra recorded from nozzle 2, Supplementary Figure S11, also show an increase in  $m/z$  42 with decreasing flow rate and a crossover point from a base peak of  $m/z$  55 to 37. Spectra recorded from nozzle 3 show a slight decrease in water cluster intensity as flow rate is decreased, and no crossover point. The distribution of clusters remains the same over the entire flow rate range, except for a slight increase in  $m/z$  42 at the lowest flow rate.

Studying the schlieren photographs of the gas profile for each nozzle reveals that nozzle 3 visually produces the most uniform gas flow profile of the four nozzles. The stability of the ion signal produced by nozzle 3 is attributed to the uniform gas flow.

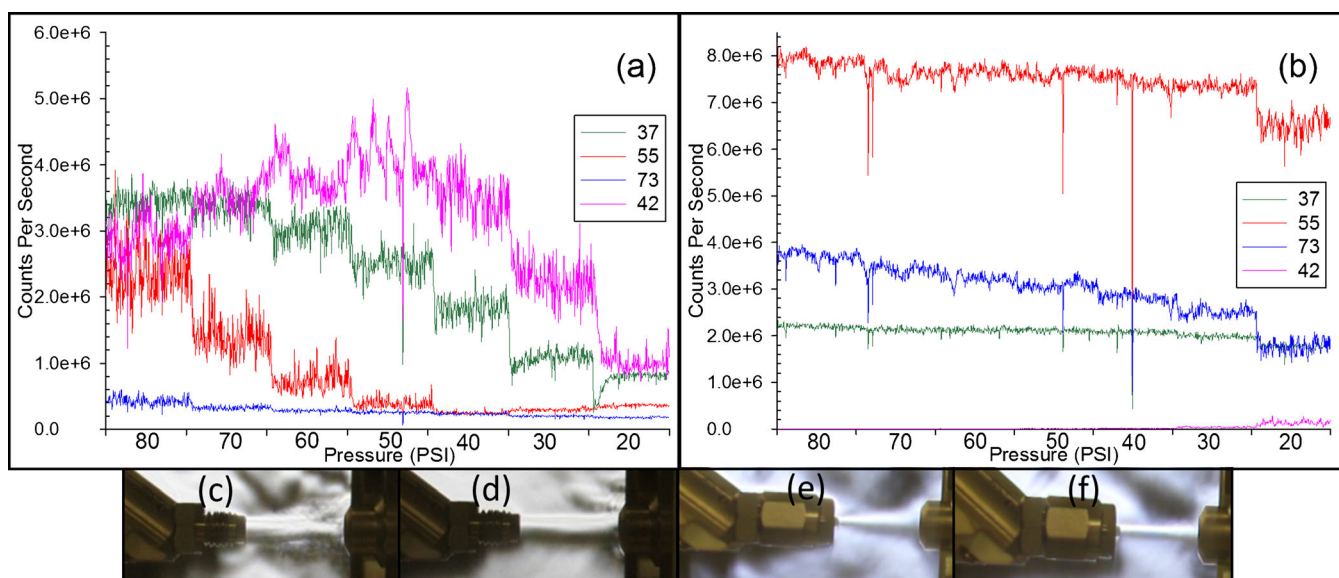


**Figure 5.** EICs for observed ions over a supplied pressure range of 80 psi to 20 psi in discrete 10 psi increments for (a) nozzle 1, 4.8 mm, (b) nozzle 3, 1.5 mm. Schlieren photographs of (c) nozzle 1 at 80 psi, (d) nozzle 1 at 20 psi, (e) nozzle 3 at 80 psi, (f) nozzle 3 at 20 psi

Nozzle 4 shows a similar consistency in ion intensity for the first three pressure data points, Supplementary Figure S13. This is followed by a rapid decrease in intensity, likely the result of poor gas flow through the nozzle at lower system pressure. EICs for nozzles 2 and 4 as well as additional schlieren photographs for all nozzles can be found in Supplementary Figures S10–S13.

## Conclusion

Smaller nozzle diameters and higher gas flow rates promote the formation of higher order water clusters and, as a result, higher bulk proton affinity of the reagent ion system. Conversely, lower flow rates and larger nozzle diameters result in lower order clusters and lower system proton affinity. By balancing gas flow rate and nozzle diameter, it may be possible to achieve some level of selectivity when using the DSA. The schlieren photographs show that as flow rate is reduced, so too is the amount of expansion of the gas flow profile. Therefore, to increase spatial resolution, smaller nozzle diameters and low flow rates should be used, although this may result in reduced sample mass transport to the mass spectrometer.

Further work is needed to determine if sample placement at the location of observed maximum water cluster intensity results in optimum analyte signal. Cluster intensity is not the only factor involved in ionization. An important factor for future investigation is the gas temperature at different regions within the gas flow profile because of its important role in the analyte desorption process leading to ionization.

## Acknowledgments

The authors thank Tim Ford, Illustrative Services Coordinator at UMBC, for help with the schlieren photography. Additionally, they thank PerkinElmer Senior Field Support Specialist, David Francis, for his help with mass spectrometry technical support.

## References

1. Takáts, Z., Cotte-Rodriguez, I., Talaty, N., Chen, H., Cooks, R.G.: Direct, trace level detection of explosives on ambient surfaces by desorption electrospray ionization mass spectrometry. *Chem. Commun.* **15**, 1950–1952 (2005)
2. McEwen, C.N., McKay, R.G., Larsen, B.S.: Analysis of solids, liquids, and biological tissues using solids probe introduction at atmospheric pressure on commercial LC/MS instruments. *Anal. Chem.* **77**, 7826–7831 (2005)
3. Cotte-Rodriguez, I., Mulligan, C.C., Cooks, R.G.: Non-proximate detection of small and large molecules by desorption electrospray ionization and desorption atmospheric pressure chemical ionization mass spectrometry: instrumentation and applications in forensics, chemistry, and biology. *Anal. Chem.* **79**, 7069–7077 (2007)
4. Yang, S., Ding, J., Zheng, J., Hu, B., Li, J., Chen, H., Zhou, Z., Qiao, X.: Detection of melamine in milk products by surface desorption atmospheric pressure chemical ionization mass spectrometry. *Anal. Chem.* **81**, 2426–2436 (2009)
5. Williams, J.P., Scrivens, J.H.: Rapid accurate mass desorption electrospray ionization tandem mass spectrometry of pharmaceutical samples. *Rapid Commun. Mass Spectrom.* **19**, 3643–3650 (2005)
6. Zhang, X., Jia, B., Huang, K., Hu, B., Chen, R., Chen, H.: Tracing origins of complex pharmaceutical preparations using surface desorption atmospheric pressure chemical ionization mass spectrometry. *Anal. Chem.* **82**, 8060–8070 (2010)
7. McEwen, C., Gutteridge, S.: Analysis of the inhibition of the ergosterol pathway in fungi using the atmospheric solids analysis probe (ASAP) method. *J. Am. Soc. Mass Spectrom.* **18**, 1274–1278 (2007)
8. Twohig, M., Shockcor, J.P., Wilson, I.D., Nicholson, J.K., Plumb, R.S.: Use of an atmospheric solids analysis probe (ASAP) for high throughput screening of biological fluids: preliminary applications on urine and bile. *J. Proteome. Res.* **9**, 3590–3597 (2010)
9. Huang, D., Luo, L., Jiang, C., Han, J., Wang, J., Zhang, T., Jiang, J., Zhou, Z., Chen, H.: Sinapine detection in radish taproot using surface desorption atmospheric pressure chemical ionization mass spectrometry. *J. Agric. Food Chem.* **59**, 2148–2156 (2011)
10. Wu, Z., Chen, H., Wang, W., Jia, B., Yang, T., Zhao, Z., Ding, J., Xiao, X.: Differentiation of dried sea cucumber products from different geographical areas by surface desorption atmospheric pressure chemical ionization mass spectrometry. *J. Agric. Food Chem.* **57**, 9356–9364 (2009)
11. Chen, H., Lai, J., Zhou, Y., Huan, Y., Li, J., Zhang, X., Wang, Z., Luo, M.: Instrumentation and characterization of surface desorption atmospheric pressure chemical ionization mass spectrometry. *Chin. J. Anal. Chem.* **35**, 1233–1240 (2007)
12. Jjunju, F.P.M., Badu-Tawiah, A.K., Li, A., Soparawalla, S., Roqan, I.S., Cooks, R.G.: Hydrocarbon analysis using desorption atmospheric pressure chemical ionization. *Int. J. Mass Spectrom.* **345/347**, 80–88 (2013)
13. Good, A., Durden, A., Kebarle, P.: Ion–molecule reactions in pure nitrogen and nitrogen containing traces of water at total pressures 0.5–4 Torr. Kinetics of clustering reactions forming  $H^+(H_2O)_n$ . *J. Chem. Phys.* **52**, 212–221 (1970)
14. Dzidic, I., Carroll, D.I., Stillwell, R.N., Horning, E.C.: Comparison of positive ions formed in nickel-63 and corona discharge ion sources using nitrogen, argon, isobutane, ammonia, and nitric oxide as reagents in atmospheric pressure ionization mass spectrometry. *Anal. Chem.* **48**, 1763–1768 (1976)
15. Froome, K.D.: The refractive indices of water vapor, air, oxygen, nitrogen and argon at 72 kMc/s. *Proc. Phys. Soc. B.* **68**, 833–835 (1955)
16. Pfeuffer, K.P., Shelley, J.T., Ray, S.J., Hieftje, G.M.: Visualization of mass transport and heat transfer in the FAPA ambient ionization source. *J. Anal. At. Spectrom.* **28**, 379–387 (2013)
17. Pfeuffer, K.P., Schaper, J.N., Shelley, J.T., Ray, S.J., Chan, G.C.Y., Bings, N.H., Hieftje, G.M.: Halo-shaped flowing atmospheric pressure afterglow: a heavenly design for simplified sample introduction and improved ionization in ambient mass spectrometry. *Anal. Chem.* **85**, 7512–7518 (2013)
18. Pfeuffer, K.P., Ray, S.J., Hieftje, G.M.: Measurement and visualization of mass transport for the flowing atmospheric pressure afterglow (FAPA) ambient mass-spectrometry source. *J. Am. Soc. Mass Spectrom.* **25**, 800–808 (2014)
19. Keelor, J.D., Dwivedi, P., Fernández, F.M.: An effective approach for coupling direct analysis in real time with atmospheric pressure drift tube ion mobility spectrometry. *J. Am. Soc. Mass Spectrom.* **25**, 1538–1548 (2014)
20. Hosch, J.W., Walters, J.P.: High spatial resolution schlieren photography. *Appl. Opt.* **16**, 473–482 (1977)
21. Settles, G.S.: *Schlieren and shadowgraph techniques: visualizing phenomena in transparent media*, 1st edn. Springer-Verlag, Germany (2001)
22. Cheng, H.P.: Water clusters: fascinating hydrogen-bonding networks, solvation shell structures, and proton motion. *J. Phys. Chem. A.* **102**, 6201–6204 (1998)
23. Kawai, Y., Yamaguchi, S., Okada, Y., Takeuchi, K., Yamauchi, Y., Ozawa, S., Hiromi, N.: Reactions of protonated water clusters  $H^+(H_2O)_n$  ( $n = 1–6$ ) with dimethylsulfoxide in a guided ion beam apparatus. *Chem. Phys. Lett.* **377**, 69–73 (2003)
24. Wróblewski, T., Ziemczonek, L., Karwasz, G.P.: Proton transfer reactions for ionized water clusters. *Czech J. Phys.* **54**, C747–C752 (2004)
25. Hunter, E.P.L., Lias, S.G.: Evaluated gas phase basicities and proton affinities of molecules: an update. *J. Phys. Chem. Ref. Data* **27**, 414–656 (1998)